ELSEVIER

Carbohydrate Research 336 (2001) 297–308

CARBOHYDRATE RESEARCH

www.elsevier.com/locate/carres

Two stereoisomeric $3^{I},2^{II}$-anhydro-α-cyclodextrins: a molecular dynamics and crystallographic study☆

Stefan Immel,[a,*] Kahee Fujita,[b] Makoto Fukudome,[b] Michael Bolte[c,†]

[a]*Institut für Organische Chemie, Technische Universität Darmstadt, Petersenstraße 22, D-64287 Darmstadt, Germany*

[b]*Faculty of Pharmaceutical Sciences, Nagasaki University, 1-14 Bunkyo-machi Nagasaki 852-8521, Japan*

[c]*Institut für Organische Chemie, J.W. Goethe-Universität Frankfurt, Marie-Curie-Straße 11, D-60439 Frankfurt (Main), Germany*

Received 10 August 2001; accepted 8 October 2001

Abstract

Regioselective epoxide ring opening of $2^{I},3^{I}$-($2^{I}S$)-anhydro-α-cyclodextrin (**1**) through intramolecular attack of hydroxyl groups of neighboring glucose rings occurs in diequatorial fashion to yield $3^{I},2^{II}$-anhydro-α-cyclodextrin (**3**) with a rigid glucopyranose–dioxane–glucopyranose tricyclic ring system, the usual diaxial opening and the gluco/altro-configurated stereoisomer **2** cannot be detected. Molecular dynamic simulations in water were used to analyze the conformations of **1**–**3** and the stereochemical implications of this reaction. Due to the contracted 2,3-OH side of the torus, **3** features an inverted conicity compared to the parent α-cyclodextrin. A crystallographic study on the bis-**3**·3 *n*-PrOH nonahydrate not only displays little variations between the solid-state and solution geometries of **3**, but also provides a molecular picture of a unique inclusion complex in which three *n*-propanol molecules are distributed in the cavity of a dimeric unit of **3** (monoclinic, space group $P2_1$, $a = 14.257(1)$, $b = 22.623(2)$, $c = 16.644(1)$ Å, $\beta = 104.82(1)°$, all 19278 reflections with $I > 2\sigma(I)$ yield $R(F) = 0.1017$).

Keywords: $2^{I},3^{I}$-($2^{I}S$)-Anhydro-α-cyclodextrin; $3^{I},2^{II}$-Anhydro-α-cyclodextrin; Molecular dynamics; Crystal structure; *n*-Propanol inclusion complex

1. Introduction

Cyclodextrin (CD) 2,3-*manno*-epoxides[2–10] are highly useful intermediates in the course of chemical transformations of the backbone structure of these macrocycles.[11,12] In general, epoxide ring opening occurs highly selectively through nucleophilic attack in a trans-diaxial type fashion at C-3, offering versatile synthetic routes towards, e.g., per-3-deoxy-cyclomannans,[13] mono-*altro*-CDs,[14–16] di-*altro*-CDs,[17] and cycloaltrans (α-, β-, and γ-'cycloaltrin'),[18–22] although the alternative diequatorial ring opening at C-2 has also been observed to occur to a lesser extent for various sulfur- and nitrogen-containing nucleophiles.[23] It therefore may be surmised, that intramolecular variations of this reaction proceed with similar stereo- and regioselectivity. In the case of $2^{I},3^{I}$-($2^{I}S$)-anhydro-α-CD (**1**), the in-

☆ Molecular modeling of saccharides, Part 30. For Part 29, see Ref. 1.

* Corresponding author. Tel.: +49-6151-165277; fax: +49-6151-166674.

E-mail address: lemmi@sugar.oc.chemie.tu-darmstadt.de (S. Immel).

† X-ray analysis, solution, and refinement.

0008-6215/01/$ - see front matter

PII: S0008-6215(01)00267-1

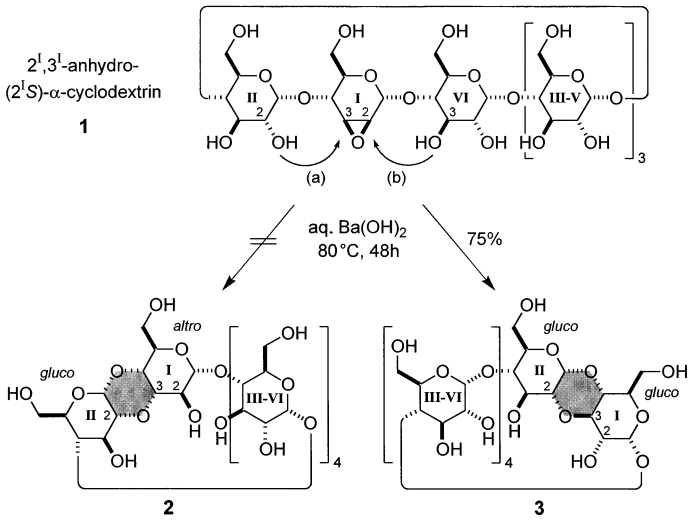

Scheme 1. Competing pathways (a) and (b) for the intramolecular ring opening of the mono-epoxide of α-cyclodextrin **1** through attack of neighboring hydroxyl groups (along pathway (b) the labeling of the sugar units changes).

tramolecular attack on the epoxide can involve either the 2^{II}-OH or 3^{VI}-OH group of the adjacent glucose residues (cf. Scheme 1). Along pathway (a), the trans-diaxial type opening leaves the pyranoid ring I with altro-configuration, whereas the alternative reaction path (b) generates a glucopyranoid ring I (diequatorial epoxide opening). Unexpectedly, the base-induced formation of the 1,4-dioxane ring exclusively proceeds via pathway (b), i.e. **1** → **3**, the formation of **2** was not observed.[24]

As an interpretation of this finding, it was brought forth that the trans-diaxial opening of the epoxide is sterically hindered by the macrocyclic structure of the CD derivative.[24] Although flexible CD derivatives or non-glucose cyclooligosaccharides[25] receive interest in mimicking the induced-fit type molecular recognition[16] by enzymes,[26] a study on the binding ability of methyl orange towards a number of CDs with deformed cavities indicated that the higher homolog of **3**, i.e. $3^{I},2^{II}$-anhydro-β-CD (**4**) is the only candidate amongst the compounds studied to exhibit stronger binding (by about a factor of 2.8 at 10 °C) than β-CD itself.[27] In this context of rigidified, lock-and-key type[28] hosts with increased affinity towards guest molecules, we here report on the molecular structures and conformations of the compounds involved in the formation of $3^{I},2^{II}$-anhydro-CDs, based on a molecular modeling study in conjunction with a crystallographic analysis of **3**.

2. Results and discussion

Although compounds **2** and **3** result from different regioselectivities in the course of epoxide ring opening, both are in fact stereoisomers rather than regioisomers due to the symmetry of the macrocycle. In **2**, a cis–cis type junction of a glucopyranoid ring and an altropyranose is realized via a central 1,4-dioxane ring (cf. Scheme 2). As altrose itself exhibits considerable intrinsic flexibility in which the ring adopts either a $^4C_1$ chair or an

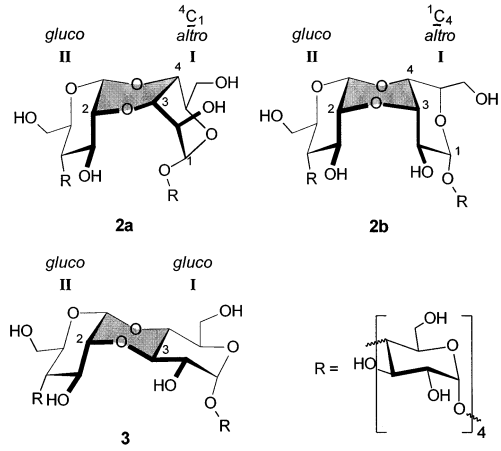

Scheme 2. Molecular configurations and possible conformations of $3^{I},2^{II}$-anhydro-α-cyclodextrin: trans-diaxial epoxide ring opening (**1** → **2**, pathway (a) in Scheme 1) conceivably results in two conformers with the altropyranose residue I adopting either the $^4C_1$ (**2a**) or $^1C_4$ (**2b**) geometry. Through the alternative pathway (b) both pyranose rings retain gluco-configuration (**1** → **3**). The central dioxane ring of each compound is highlighted by shading.

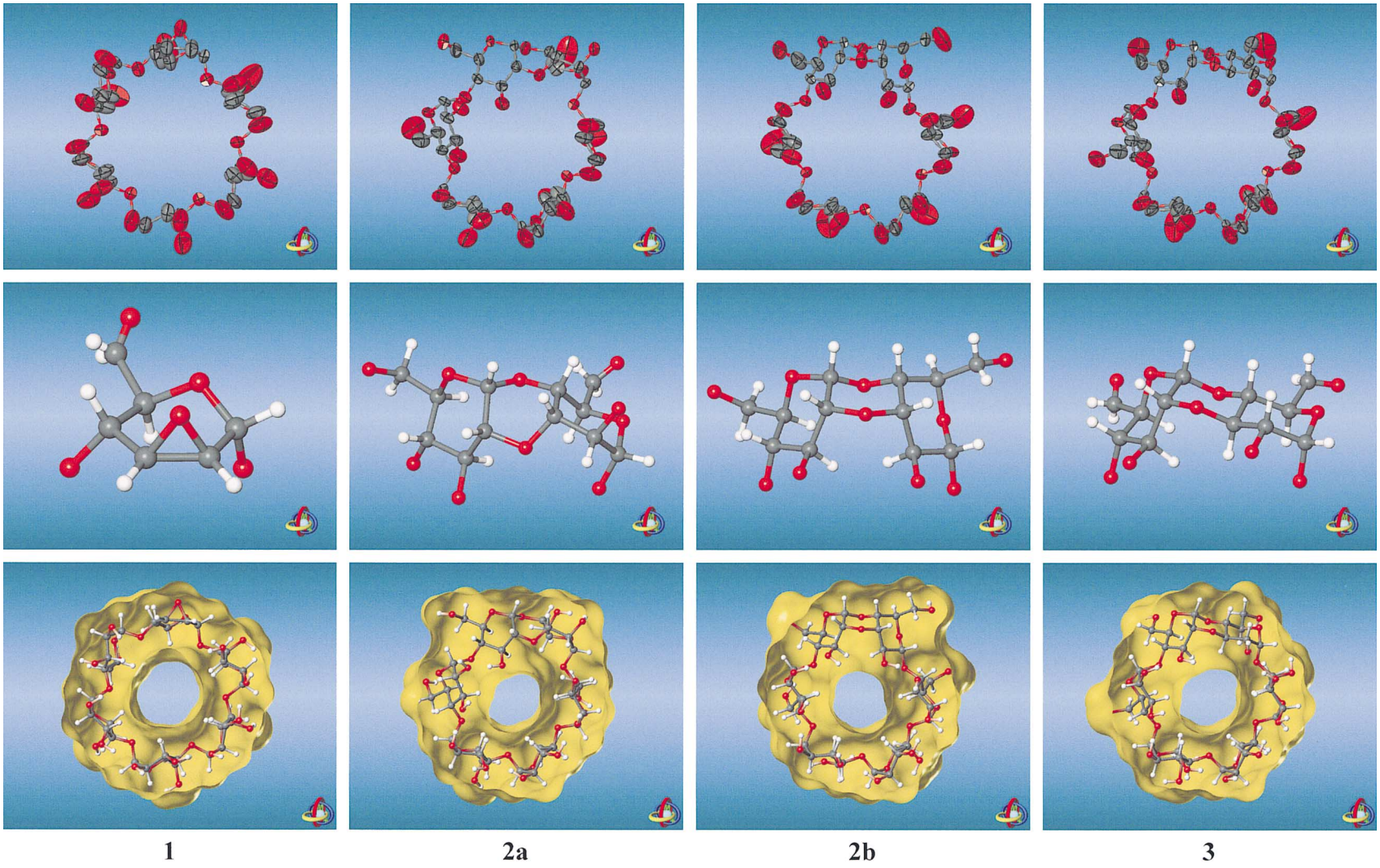

Fig. 1. Mean molecular geometries (heavy atom positions only) and anisotropic thermal ellipsoids (top row) of $2^{I},3^{I}$-anhydro-($2^{I}S$)-α-CD (**1**) and the isomeric $3^{I},2^{II}$-anhydro-α-CDs (**2a**, **2b**, and **3**) as derived from MD simulations in water. Center row: Enlarged ball-and-stick-type model of the sugar 2,3-epoxide unit in **1** (left) and the $3^{I},2^{II}$-anhydro units in **2a** and **2b** (gluco/altro-configuration) as well as of **3** (gluco/gluco-stereoisomer); hydroxyl-hydrogen atoms are omitted due to their flexibility. Bottom: Solvent-accessible surface models (yellow) of typical snapshot geometries extracted from the MD trajectories displaying the distorted ring conformations of the macrocycles. All molecular orientations correspond to each other, the center row models represent the topmost sugar units in the macrocycles, respectively.

Table 1
Cremer–Pople puckering parameters (Q, Θ, and ϕ),[37,38] ring conformations, and tilt angles τ[39] for the pyran and dioxane rings of **1**–**3** (MD-derived averages with root-mean-square deviations in parentheses)

Compound	Ring	Configuration	Q (Å) [a]	Θ (°) [a]	ϕ (°) [a,b]	Conformation	Tilt τ (°) [c]
1	I	manno	0.557(33)	50.9(5.4)	353(10.0)	${}^{O}H_5$ ($\rightarrow {}^{O}E$)	100(12)
	II–VI [d]	gluco	0.620(29)	14.9(5.4)	38(24.3)	${}^{4}C_1$	94(12)
2a	I	altro	0.588(29)	19.2(4.9)	356(18.1)	${}^{4}C_1$	97.4(6.7)
	dioxane		0.759(37)	87.4(2.9)	136.3(5.5)	${}^{O4,C4}B$	56.7(5.3)
	II	gluco	0.613(30)	14.0(5.2)	316(26.2)	${}^{4}C_1$	30.4(4.8)
	III–VI [d]	gluco	0.625(29)	15.1(5.9)	36(26.0)	${}^{4}C_1$	86(15)
2b	I	altro	0.575(33)	171.5(4.8)	190(74.0)	${}^{1}C_4$	56.0(6.2)
	dioxane		0.547(30)	156.2(5.1)	187(16.5)	${}^{O3}C_{O4'} \leftrightarrow {}^{C4}H_{O4}$	67.7(6.0)
	II	gluco	0.597(31)	16.2(5.8)	331(25.5)	${}^{4}C_1$	59.2(6.1)
	III–VI [d]	gluco	0.624(29)	16.5(5.9)	43(21.4)	${}^{4}C_1$	88.0(9.2)
3	I	gluco	0.647(28)	6.4(3.2)	37(65.9)	${}^{4}C_1$	68.3(5.7)
	dioxane		0.589(29)	171.7(3.8)	242(51.4)	${}^{O3}C_{O4'}$ [e]	70.9(5.3)
	II	gluco	0.618(30)	10.8(4.6)	342(36.3)	${}^{4}C_1$	50.2(5.1)
	III–VI [d]	gluco	0.623(29)	15.4(5.0)	40(21.2)	${}^{4}C_1$	89(12)

[a] Ring numbering scheme for pyranoses: O-5–C-1–C-2–C-3–C-4–C-5; dioxane rings: O-4–C-4–C-3–O-3–C-2′–C-1′.
[b] For $\Theta \rightarrow 0°$ (${}^{4}C_1$) and $\Theta \rightarrow 180°$ (${}^{1}C_4$), the parameter ϕ becomes insignificant.
[c] Angle between the least-squares best-fit mean plane of the macrocycle (defined by all intersaccharidic O-4 atoms) and the mean plane of the pyranose or dioxane rings; values of $\tau < 90°$ indicate inward tilting of the C-2 and C-3 side of the pyranoses.
[d] Combined averages for all unmodified glucopyranose rings in the macrocycle.
[e] ${}^{O3}C_{O4'} \equiv {}^{O3}C_{O4} \equiv {}^{C1'}C_{C3}$.

inverted ${}^{1}C_4$ chair geometry with almost equal energies,[20–22,25,29] two different conformers **2a** and **2b** need to be considered. In contrast, the tricyclic pyran–dioxane–pyran system in **3** features a rigid cis–trans type linkage, allowing for standard chair conformations of all six-membered rings. Similar arrangements are observed in the class of spectinomycin antibiotics and related compounds.[30]

Molecular dynamic simulations.—A detailed conformational analysis of the structures of **2a**, **2b**, and **3** was carried out using independent molecular dynamic (MD) simulations with the explicit incorporation of water as the solvent (cf. Section 4); for comparison, their common precursor **1** was also included in this study. In each case, constant temperature ($T \approx 300$ K) and constant pressure ($P \approx 1$ bar) MD trajectories of 1 ns length were generated on periodic boxes (truncated octahedron) filled with the solute and a total of 609 TIP3-type water molecules, using CHARMM[31,32] and a force-field adapted to properly treat carbohydrate structures.[33,34] The MD-derived mean-solute structures, their thermal-displacement ellipsoids, as well as solvent-accessible surface[35,36] models of typical solution snapshot geometries are displayed by Fig. 1. Not unexpectedly, all macrocyclic structures are characterized by rather limited flexibility of their backbones, with only the 2-OH, 3-OH, and 6-CH_2OH groups undergoing significant torsional transitions. In particular, neither MD run on conformers **2a** and **2b** displays any interconversion between these forms, both apparently being too rigid to equilibrate on the MD time scale.

Particular emphasis was put on the analysis of the pyranose and dioxane ring portions of **1**–**3** in terms of their geometries and their relative alignments. Table 1 gives a detailed listing of their Cremer–Pople puckering parameters[37,38] for all six-membered rings. The combined averages over all glucopyranoses (rings II–VI in **1**, and III–VI in **2a**, **2b**, and **3**) correlate with their generally favored ${}^{4}C_1$ conformations (Θ less equal approx. 16°), significant deviations are only observed for the anhydro-residues. Due to the epoxide, the ring I in **1** (Fig. 1, center row, left) adopts a typical ${}^{O}H_5$ half-chair geometry (slightly distorted towards an ${}^{O}E$ envelope), which agrees well with previous crystallographic studies on inclusion complexes of 2,3-*per*-anhydro-α-cycloman-

nan[6,7] and other related sugar epoxides[40] contained in the Cambridge Crystallographic Database.[41,42]

As was already deduced from the formula drawing of Scheme 2, the cis–trans linked tricyclic system in **3** consists of rigidly anellated, almost relaxed chair-type rings even for the center dioxane portion. Significant distortions of the dioxane ring are observed for **2a** and **2b** with the ring I of the altropyranose residue adopting either the $^4C_1$ (ideal values of $\Theta \approx 0°$) or $^1C_4$ ($\Theta \approx 180°$) form. In **2a**, the cis–cis-type junction forces the center ring into a strained boat form, simultaneously transferring some energy into distortions of the altrose ring I as evidenced by the rather large value of $\langle \Theta \rangle = 19.2°$. Most notably, a similar boat conformation was found for the center dioxane ring in the X-ray structure of cyclobis-(1→2)-α-D-glucopyranosyl peracetate.[43] For **2b**, the close spatial proximity of both axially disposed H-2^{I} (altrose) and H-3^{II} (glucose) protons (Fig. 1) pointing towards each other excerpts considerable strain on the center dioxane ring, which is therefore flattened (lowest puckering amplitude Q of all rings) and distorted towards a half-chair.

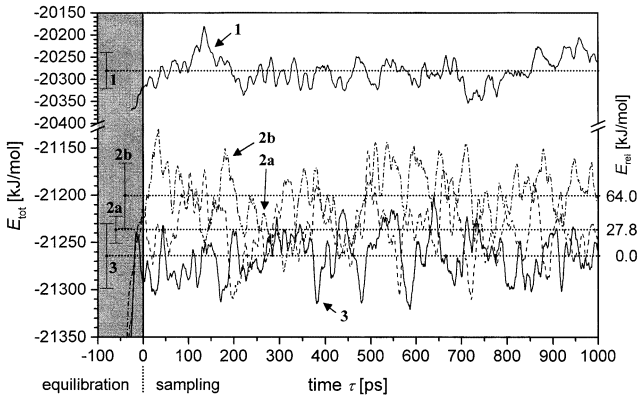

Fig. 2. Time series of total energies during the MD simulations of **1**, **2a**, **2b**, and **3** in periodic boxes (truncated octahedron) filled with 609 H_2O molecules (all box sizes approx. 33.5 ± 0.1 Å, $\langle T \rangle = 295.3$ K, $\langle P \rangle = 1$ bar), respectively, plotted as running averages smoothed over 100 configurations (5 ps) each. Negative times ($\tau = -100 - 0$ ps) indicate the equilibration phase, followed by a total data acquisition period of 1 ns. The average energies and the corresponding root-mean-square fluctuations of the energies during the sampling simulation are indicated by the dotted lines and the error bars on the left. Besides indicating the completed equilibration of all MD systems, the two conformers **2a** and **2b** appear to be 27.8 and 64.0 kJ/mol less stable than their stereoisomer **3**.

The overall molecular shape of cyclodextrins is characterized by the tilt angle τ formed between both the plane of the macrocycle and the ring plane of each sugar unit.[39] In general, the glucose units of unmodified CDs and their inclusion complexes are slightly tilted with their 6-CH_2OH groups pointing towards the central molecular axis, and thus the 2- and 3-OH groups form the wider opened aperture of these truncated cone-type structures.[39,44,45] A similar trend is observed for **1** as evidenced by tilt angles larger than 90° (cf. Table 1). However, the strait-jacket of the $3^{I},2^{II}$-anhydro linkage in **2** and **3** leads to a considerable contraction along this torus rim: the unmodified glucose residues (rings III–VI) are aligned almost perpendicular to the macroring, whereas the rings I and II, as well as the center dioxane unit, display severe misalignments with pronouncedly decreased and inverted inclinations. The effects of very low tilt angles on the backbone structures of **1**–**3** become particularly evident from the solid-surface models given in Fig. 1: of all structures, both conformers **2a** and **2b** exhibit the most asymmetrically distorted over-all shapes.

The relative stabilities of the conformers **2a** and **2b** and their stereoisomer **3** are expressed in the MD-derived averages of the total energies of the simulation system, a cautious analysis made possibly by identical simulation parameters (i.e. equal temperature, pressure, box size, number of water molecules, constant set of force-field parameters, long simulation periods), despite the lack of direct conformational transitions in either unconstrained (free) or constrained (chemical or structural perturbation) form. From the plot of the total energies ($E_{kin} + E_{pot}$) of the MD systems given in Fig. 2, **3** turns out as the energetically most favorable structure, whereas **2a** and **2b** appear to be—within the limits of error—about 28 and 64 kJ/mol higher in average total energy. As deduced above, the main reasons for these relative stabilities seem to originate from strain within the cis–trans (**3**) versus cis–cis (**2a**, **2b**) type linkages in the tricyclic system and their alignments in the macrocycle.

Obviously, **3** is the thermodynamically most favored product emerging from intramolecular ring opening of the epoxide in **1**. An

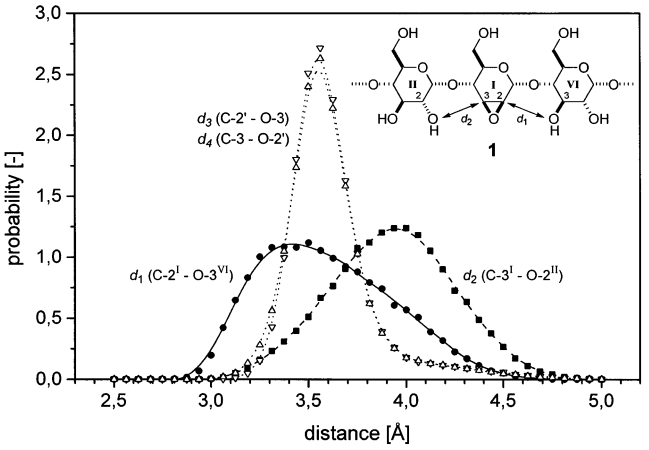

Fig. 3. Probability distributions of intramolecular distances between epoxide ring carbon atoms C-2^{I} and C-3^{I} and neighboring hydroxyl oxygen atoms O-3^{VI} and O-2^{II} as obtained from MD simulations of **1** in water. The distribution of d_1 (C-2^{I}···O-3^{VI}, solid line and circles) is significantly shifted towards lower distances as compared to d_2 (C-3^{I}···O-2^{II}, dashed line and squares), apparently favoring intramolecular attack of the 3^{VI}-OH group (**1**→**3**) over the 2^{II}-OH hydroxyl (**1**→**2**) onto the epoxide. For comparison, the distributions d_3 and d_4 of the C-2′···O-3 and C-3···O-2′ interresidue distances averaged over all neighboring unmodified glucose portions were included (triangles and dotted lines).

indication that **3** is also the kinetically preferred product of this reaction can be deduced from the comparison of intramolecular distances between the epoxide ring carbon atoms and neighboring hydroxyl oxygens suitable for attack: the probability distributions plotted in Fig. 3 display significantly shorter distances between the epoxide carbon C-2^{I} and O-3^{VI} ($\langle d_1 \rangle = 3.59(34)$ Å) as compared to C-3^{I} and O-2^{II} ($\langle d_2 \rangle = 3.93(32)$ Å), favoring the reaction **1**→**3** rather than **1**→**2**. That this effect is indeed caused by the $^{O}H_5$ ring conformation of the 2,3-anhydro-*manno*-epoxide unit within the macrocycle is displayed by the rather equal and uniform distances C-2′···O-3 and C-3···O-2′ between all unmodified glucose units ($\langle d_3 \rangle \approx \langle d_4 \rangle \approx 3.62$ Å).

Crystallographic analysis.—Precipitation of **3** from aqueous *n*-propanol yielded crystals suitable for X-ray analysis, and thus allows comparison of its solid-state structure with the MD-derived conformation in solution. The low-temperature ($T = 173$ K) structure analysis revealed a composition of bis-(3^{I},2^{II}-anhydro)-α-cyclodextrin (**3**)·3 *n*-PrOH·9 H_2O of the block-shaped, monoclinic crystals with space group $P2_1$ (cf. Fig. 4).

The CD hosts are stacked in parallel columns in an alternating head-to-head and tail-to-tail fashion. The *n*-propanol guest molecules are all located within the almost linear, nano-tube like channels formed by the columnar CD arrangement, whereas the water molecules are located without exception on interstitial positions outside of the macrocycles. As evidenced by their rather large displacement ellipsoids (Fig. 4, top left), the guest molecules retain some considerable degree of disorder even at low temperatures. As is typically observed for glucopyranose residues, all 6-CH_2OH groups on the CD hosts are twofold disordered over gauche–gauche (*gg*) and gauche–trans (*gt*) orientations, the former being favored over the latter by a ratio of 7.67:4.33 (calculated from the occupancy factors of all 12 O-6 positions included in the asymmetric unit).

The crystal architecture displays an intensive three-dimensional hydrogen bonding network, in which all hydroxyl groups and water molecules are involved; a schematic drawing is given in Fig. 5 and some distances are listed in Table 2. From the different types of hydrogen bonds observed—i.e. CD···CD intramolecular (O-3′···O-2) and intermolecular H-bonds, CD···water, water···water, CD···*n*-propanol and *n*-propanol···*n*-propanol—it is obvious that the guest molecules are not hydrogen bonded to any of the water molecules, but are shielded by their macrocyclic hosts from the water positions in the crystal environment. Of the three *n*-propanol contained in the asymmetric unit of the lattice, one is twofold H-bonded to O-2 and O-3′ of the anhydro-glucopyranose portion of one molecule **3** (hydrogen bonds labeled 14 and 15 in Fig. 5 and Table 2). The remaining two *n*-propanol face each other in a head-to-head like arrangement interacting through their hydroxyl groups (H-bond no. 16); a detailed plot of this configuration is provided in Fig. 5 by the slices through the corresponding molecular surfaces. Obviously, the tube-like cavity of a dimeric unit of **3** in the crystal lattice is perfectly able to accommodate the three guest molecules *n*-PrOH with their arrangement being determined through the necessity to satisfy their hydrogen bonding requirements.

As the most characteristic feature of **3**, its ribbon model displays the significant contraction along the front aperture of the torus carrying the 2- and 3-OH groups. The unusual conicity of this CD derivative expresses itself in rather low tilt angles τ for the $3^{I},2^{II}$-anhydro-ring system ($\tau \approx 60°$, cf. Table 3), in contrast to unmodified CDs where the 6-CH_2OH side invariably represents the narrower opening ($\tau > 100°$)[39] of these truncated cone structures. As was already deduced for the MD derived geometry of **3**, the pyranose and dioxane rings adopt standard chair conformations within their rather rigid link-ups (cf. Cremer–Pople parameters[37,38] listed in Table 3). Indeed, both independently derived structures of **3** for the crystal and solution state feature identical over-all shapes, their backbones (heavy atoms including all substituents except the O-6 atoms) being superimposable with average deviations in their atomic positions of less than 0.1 Å. Obviously, the crystal conformation of **3** undergoes no significant changes upon dissolution in water.

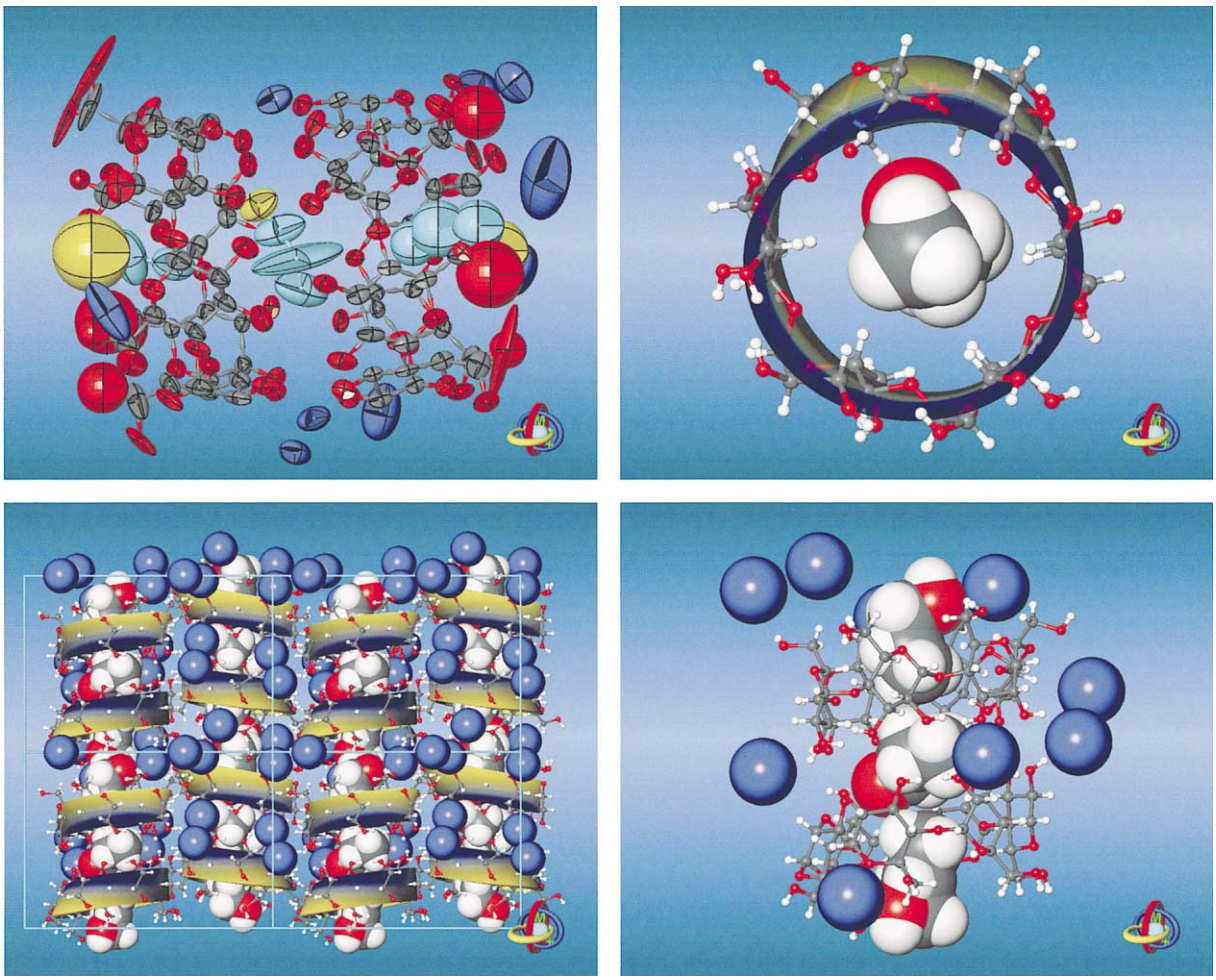

Fig. 4. Solid-state structure of $3^{I},2^{II}$-anhydro-α-cyclodextrin (**3**). Top left: Molecular geometry and 50% thermal ellipsoids of the asymmetric unit ([**3**]$_2$·3 *n*-PrOH·9 H_2O); for clarity, the water oxygen atoms are colored dark blue and the *n*-propanol guests are displayed in yellow (oxygens) and cyan (carbon atoms). Top right: Single complex extracted from the asymmetric unit, the semi-transparent ribbon-model shows the distorted conicity of the host molecule (blue, ring side carrying the 2- and 3-OH groups; yellow, 6-CH_2OH) with the *n*-propanol guest (CPK model) centered along its central axis (view perpendicular to the ring plane of **3**). Bottom left: Crystal lattice (1·2·2 unit cells, view down the *a*-axis) made up of columnar head-to-head and tail-to-tail stacked anhydro-CDs (ribbon models) including almost linear and parallel assemblies of *n*-propanol guest molecules (CPK models); the guest–host arrangement being surrounded by water molecules (blue spheres) in the crystal. Bottom right: Section extracted from the lattice, displaying in detail the alignment of three guest molecules in a dimeric unit of **3**. For all ball-and-stick type models of **3** only the preferably occupied configurations of all disordered 6-CH_2OH groups were retained for the graphics.

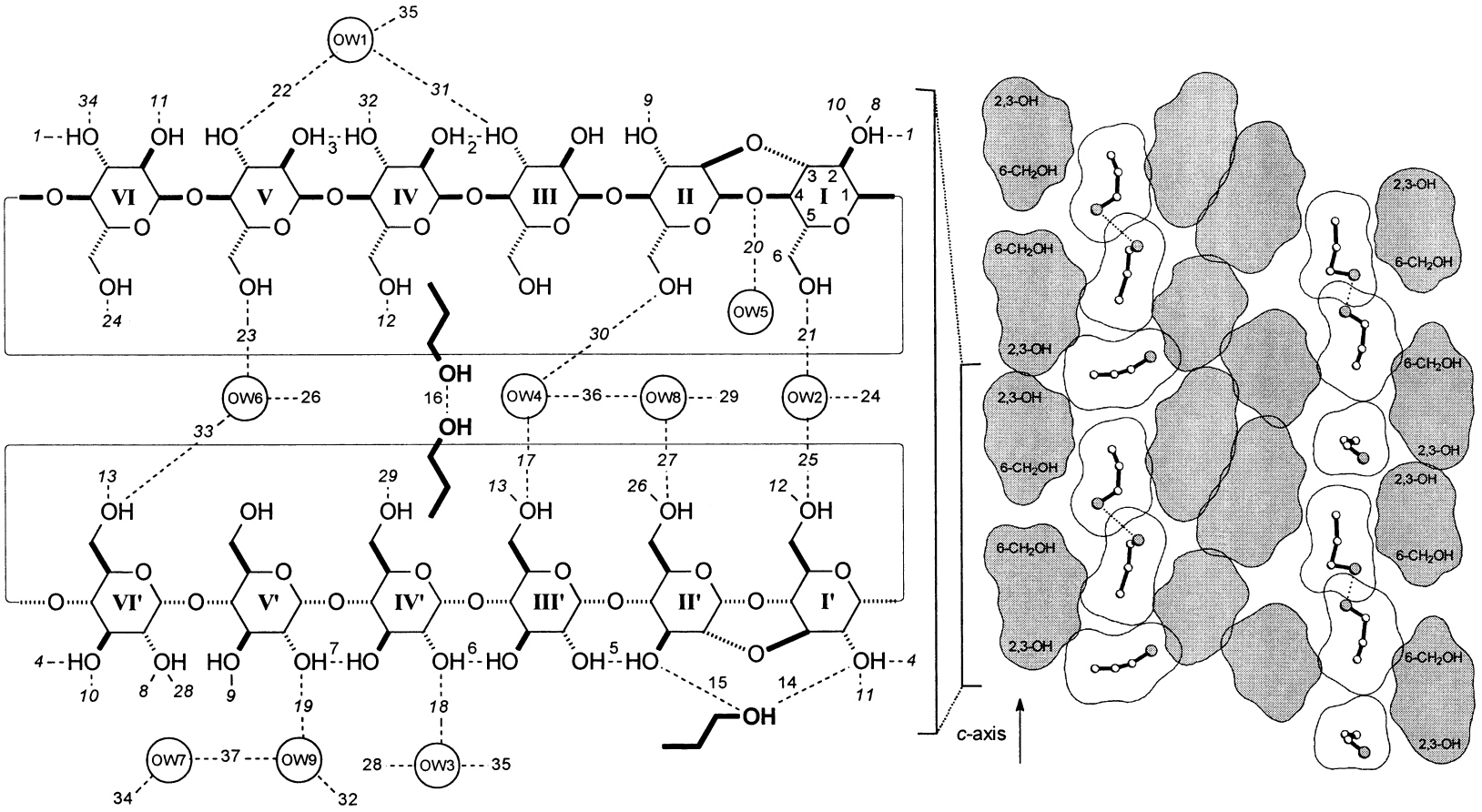

Fig. 5. Scheme of intra- and intermolecular hydrogen bonds in the solid-state structure of the bis-(3^{I},2^{II}-anhydro)-α-CD–**3**·*n*-propanol nonahydrate inclusion complex (left). The individual glucose units within the asymmetric unit are labeled I–VI and I′–VI′, the water molecules OW1–OW9, the numbers in italics correspond to the indices given in Table 3. On the right, a larger segment of the crystal (four asymmetric units) displays the nano-tube like environment of stacked CD hosts into which the *n*-propanol guest molecules are embedded (water molecules omitted for clarity). The surface slices are given for the individual molecules, ball-and-stick type models without hydrogens are shown for *n*-propanol only, the CD surfaces are indicated by shading; dotted lines indicate hydrogen bonds between the guest molecules.

Table 2
Hydrogen bonds in the solid-state structure of bis-**3**·3 *n*-PrOH·9 H_2O, listed for acceptor···donor distances < 3.2 Å; the water molecules are labeled OW1–OW9, the glucose labeling I–VI, I′–VI′, and the indices given in the first column correspond to Fig. 5

		Distance	Symmetry			Distance	Symmetry
CD–CD intramolecular:				*CD–water*:			
1	$O(3^{VI})\cdots O(2^{I})$	2.753	a	17	$O(6^{III'})\cdots O(W4)$	2.826	a
2	$O(2^{IV})\cdots O(3^{III})$	2.988	a	18	$O(2^{IV'})\cdots O(W3)$	2.721	a
3	$O(2^{V})\cdots O(3^{IV})$	2.905	a	19	$O(2^{V'})\cdots O(W9)$	2.700	a
4	$O(3^{VI'})\cdots O(2^{I'})$	2.789	a	20	$O(4^{I})\cdots O(W5)$	3.013	b
5	$O(3^{II'})\cdots O(2^{III'})$	2.865	a	21	$O(6^{I})\cdots O(W2)$	2.626	b
6	$O(3^{III'})\cdots O(2^{IV'})$	2.776	a	22	$O(3^{V})\cdots O(W1)$	2.847	b
7	$O(3^{IV'})\cdots O(2^{V'})$	2.815	a	23	$O(6^{V})\cdots O(W6)$	2.993	b
CD–CD intermolecular:				24	$O(6^{VI})\cdots O(W2)$	2.709	b
8	$O(2^{I})\cdots O(2^{VI'})$	2.946	b	25	$O(6^{I'})\cdots O(W2)$	2.222	b
9	$O(3^{II})\cdots O(3^{V'})$	2.842	b	26	$O(6^{II'})\cdots O(W6)$	2.903	b
10	$O(2^{I})\cdots O(3^{VI'})$	2.855	b	27	$O(6^{II'})\cdots O(W8)$	2.811	b
11	$O(2^{I'})\cdots O(2^{VI})$	2.858	c	28	$O(2^{VI'})\cdots O(W3)$	2.817	d
12	$O(6^{I'})\cdots O(6^{IV})$	2.619	d	29	$O(6^{IV'})\cdots O(W8)$	2.515	f
13	$O(6^{III'})\cdots O(6^{VI'})$	2.498	e	30	$O(6^{II})\cdots O(W4)$	2.926	g
CD–propanol:				31	$O(3^{III})\cdots O(W1)$	2.879	g
14	$O(2^{I'})\cdots O(1P)$	2.787	a	32	$O(3^{IV})\cdots O(W9)$	2.827	h
15	$O(3^{II'})\cdots O(1P)$	2.766	a	33	$O(6^{VI'})\cdots O(W6)$	2.800	I
propanol–propanol:				34	$O(3^{VI})\cdots O(W7)$	2.816	j
16	O(2P)···O(3P)	3.156	b	*water–water*:			
				35	O(W1)···O(W3)	2.754	k
				36	O(W4)···O(W8)	2.082	b
				37	O(W7)···O(W9)	2.726	

Symmetry operations: (a) x, y, z. (b) $x, y, z-1$. (c) $x, y, z+1$. (d) $x-1, y, z$. (e) $x+1, y, z$. (f) $-x, y+1/2, -z-1$. (g) $-x, y+1/2, -z-2$. (h) $-x, y-1/2, -z-2$. (i) $-x-1, y+1/2, -z-1$. (j) $-x-1, y-1/2, -z-2$. (k) $-x, y-1/2, -z-1$.

Table 3
Selected geometry parameters (Cremer–Pople ring puckering parameters $Q/\Theta/\phi$,[37,38] and pyranose tilt angles τ[39]) computed for the solid-state geometry of bis-**3**·3 *n*-PrOH·9 H_2O; values are listed for both $3^{I},2^{II}$-anhydro-α-CD molecules separately (unit 1 and 2), except for the combined averages for all eight unmodified glucose residues; see also Table 1 and the comments given there

Compound	Ring	Configuration	Q (Å)		Θ (°)		ϕ (°)		Conformation	Tilt τ (°)	
			Unit 1	Unit 2	Unit 1	Unit 2	Unit 1	Unit 2		Unit 1	Unit 2
3	I	gluco	0.563	0.587	1.9	3.8	189.8	274.4	$^{4}C_{1}$	64.8	69.0
	dioxane		0.568	0.551	170.4	173.5	243.4	259.0	$^{O3}C_{O4'}$	67.8	69.9
	II	gluco	0.535	0.544	16.5	12.2	297.8	294.5	$^{4}C_{1}$	53.9	52.4
	III–VI [a]	gluco	0.557(11)		6.2(1.3)		62(18)		$^{4}C_{1}$	97.6(6.2)	

[a] Combined averages for all unmodified glucopyranose rings in both molecules of **3** with standard deviations in parentheses.

3. Conclusions

Although intramolecular opening of epoxide **1** by the 3-OH of a neighboring glucose unit occurs in an unexpected diequatorial fashion to afford **3** in high yield, MD calculations reveal **3** to be the favored product when comparing the average total energies of the stereoisomers **2a**, **2b**, and **3** in simulated water boxes. Provided that atomic distances are a decisive factor for the regioselectivity of epoxide opening, **3** also turns out to be the kinetically preferred product. The over-all molecular shape of this rigid CD derivative, as evident from its solid-state structure, not only undergoes little changes upon dissolution in

water retaining its unusual conicity caused by the contracted tricyclic pyran–dioxane–pyran ring system, but also provides a picture of an inclusion complex of **3** with *n*-propanol.

4. Experimental

Molecular dynamics simulations.—The starting geometries of **1**, **2a**, **2b**, and **3** were generated by editing the solid-state geometry of α-CD[46] and subsequent single-point energy minimization. All MD simulations starting from these structures were carried out using CHARMM[31,32] with a force-field particularly adapted for the treatment of carbohydrates[33,34] and explicit incorporation of water as the solvent. Each compound was centered in a periodic box (truncated octahedron) filled with pre-equilibrated TIP3-type water, yielding—after removal of the solvent molecules that overlap with the solute—simulation systems including 609 water molecules, respectively. After full-lattice energy minimizations, all boxes were slowly heated from 0 to 300 K within a 15 ps MD time frame, and subsequently equilibrated for an additional 85 ps; the final MD data were sampled using simulations of 1 ns in each case, molecular configurations were saved every 50 fs for analysis purposes. All MD runs were carried for constant pressure ($P_{ref} = 1$ atm, isothermal compressibility 4.63×10^{-5} atm^{-1}, pressure coupling constant $\tau_P = 5$ ps) and constant temperature ($T_{ref} = 300$ K, temperature coupling constant $\tau_T = 5$ ps, allowed temperature deviation $\Delta T = \pm 10$ K) conditions (*NPT* ensemble) using the following simulation parameters: timestep $\Delta t = 1$ fs (leap-frog integrator, all X–H bond lengths were constrained using the SHAKE protocol[47]), dielectric constant $\varepsilon = 1.0$, cut-off distance for long-range interactions 12 Å, cut-off radius for images in atom lists 13 Å; for some specific parameters recalculated from the MD trajectories see Table 4.

For each MD time series, the mean solute geometry was obtained by 3D fitting of all configurations (heavy atoms only, excluding CH_2OH-oxygen atoms); the best-fit models from this procedure were selected as representative molecular geometries in aqueous solution (Fig. 1, center and bottom row). The corresponding atomic anisotropic thermal displacement ellipsoids (cf. Fig. 1, top row) were obtained from diagonalization of the displacement tensor calculated from all atomic displacement vectors (for each atom, the eigenvectors and the root of the eigenvalues of this tensor yield the principal axis of the thermal ellipsoid and the root-mean-square atomic displacements along these directions).[48]

Crystal structure of bis-(3^I,2^{II}-anhydro)-α-cyclodextrin·3 n-*PrOH·9* H_2O.—A mixture of 60 mg of **3**, 100 μL of water and 100 μL of *n*-propanol was heated up to 90 °C to give a clear solution and then filtered through a membrane filter PTFE (pore size, 0.5 μm; TOSOH). The filtrate was sealed and allowed to stand at rt for 1 week to yield colorless, block-shaped crystals with parameters as follows: $M_r = 1126.04$ g/mol, monoclinic, space group $P2_1$, $a = 14.257(1)$, $b = 22.623(2)$, $c = 16.644(1)$ Å, $\beta = 104.82(1)°$, $V = 5189.7(7)$ Å^3, $Z = 4$, $\rho = 1.414$ g/cm, μ(Mo K_α) = 0.126

Table 4
Selected MD simulation parameters recalculated from the time series (all MD systems include 609 H_2O molecules, $M_{tot} = 11926.42$ g/mol) with standard deviations in parentheses

Compound	T [K]	E_{tot} (kJ/mol)	E_{kin} (kJ/mol)	E_{pot} (kJ/mol)	E_{rel} (kJ/mol) [a]	Box size (Å)	Volume (Å^3) [b]	Density σ (g/cm^3)
1	295.2(5.3)	−20,281(41)	4863(88)	−25,143(98)		33.47(6)	18,740(135)	1.057(8)
2a	295.3(5.3)	−21,237(14)	4864(88)	−26,101(107)	27.9	33.46(9)	18,726(142)	1.057(8)
2b	295.2(5.3)	−21,200(35)	4863(88)	−26,063(100)	64.0	33.47(6)	18,747(141)	1.056(8)
3	295.3(5.3)	−21,264(34)	4864(87)	−26,129(96)	0.0	33.47(9)	18,747(129)	1.056(7)

[a] Relative total energies for the 3^I,2^{II}-anhydro-α-cyclodextrins **2a**, **2b**, and **3** only.
[b] Volume = (box size)^3/2.0 for the truncated octahedron.

mm^{-1}, crystal dimensions $0.5 \times 0.4 \times 0.15$ mm, $T = 173(2)$ K. Of 29,184 reflections collected on a Siemens CCD three-circle diffractometer using graphite-monochromated Mo K_α ($\lambda = 0.71073$ Å) radiation, 19,278 are independent ($R_{int} = 0.0585$); θ range of data collection 1.27–28.01°, completeness to $\theta = 28.01°$ 82.4%, limiting indices h: $-16 \rightarrow 15$, k: $-28 \rightarrow 29$, and l: $-16 \rightarrow 21$. The structure was solved by shake and bake methods[49] and successive Fourier synthesis. Refinement (on F^2) was performed by full-matrix least-squares method (19,278 reflections, 18 restraints, 1403 independent parameters).[50] $R(F) = 0.1017$ for reflections with $I > 2\sigma(I)$, $wR(F^2) = 0.2193$ for 19,278 reflections ($w = 1/[\sigma^2(F_o^2) + (0.1337P)^2 + 4.1868P$); where $P = (F_o^2 + 2F_c^2)/3$); $R(F) = 0.2205$ and $wR(F^2) = 0.2966$ for all reflections. The final goodness-of-fit on F^2 equals 1.005, the largest difference peak and hole of electron density are $+0.503$ and -0.296 e Å^3, respectively. All bond length and angles fall within normal ranges for carbohydrate structures.

All 6-CH_2OH groups on both cyclodextrin units are twofold disordered over the gauche–gauche (*gg*, torsion angle ω O_5–C_5–C_6–O_6 approx. $-60°$) and the gauche–trans (*gt*, $\omega \approx +60°$) orientation, with the former being favored over the latter by a ratio of 7.67:4.33 based on relative occupancy factors. All non-hydrogen atoms (except of one *n*-propanol molecule and eight of the 12 O-6 position with lower occupancy) were refined anisotropically, hydrogen atoms were positioned geometrically and considered in calculated positions with the $1.2U_{eq}$ value of the corresponding bound atom. The ribbon models of **3** (Fig. 4) were computed by connecting the centers and normal vectors of the least-squares best-fit mean planes of all pyranose rings (without substituents) via cubic splines.[48]

5. Supplementary material

Crystallographic data (excluding structure factors) for the structure in this paper have been deposited with the Cambridge Crystallographic Data Centre as supplementary publication no. CCDC-168467. Copies of the data can be obtained, free of charge, on application to The Director, CCDC, 12 Union Road, Cambridge CB2 1EZ, UK, (fax: +44-1223-336033 or e-mail: deposit@ccdc.cam.ac.uk or www: http://www.ccdc.cam.ac.uk).

Acknowledgements

The authors are grateful to Professor F.W. Lichtenthaler (S.I.) for prolific discussions and carefully editing the manuscript, and Professor H.J. Lindner (M.B.) for lucid suggestions.

References

1. Immel, S.; Lichtenthaler, F. W.; Lindner, H. J.; Nakagawa, T. *Tetrahedron: Asymmetry* **2001**, *12*, in press.
2. Fujita, K.; Nagamura, S.; Imoto, T. *Tetrahedron Lett.* **1984**, *25*, 5673–5676.
3. Ikeda, H.; Nagano, Y.; Du, Y.; Ikeda, T.; Toda, F. *Tetrahedron Lett.* **1990**, *31*, 5045–5048.
4. Coleman, A. W.; Zhang, P.; Ling, C. C.; Mahuteau, J.; Parrot-Lopez, H.; Miocque, M. *Supramol. Chem.* **1992**, *1*, 11–14.
5. Zhang, P.; Coleman, A. W. *Supramol. Chem.* **1993**, *2*, 255–263.
6. Immel, S.; Fujita, K.; Lindner, H. J.; Nogami, Y.; Lichtenthaler, F. W. *Chem. Eur. J.* **2000**, *6*, 2327–2333.
7. Immel, S.; Lichtenthaler, F. W.; Lindner, H. J.; Fujita, K.; Fukudome, M.; Nogami, Y. *Tetrahedron: Asymmetry* **2000**, *11*, 27–36.
8. Khan, A. R.; Barton, L.; D'Souza, V. T. *J. Chem. Soc., Chem. Commun.* **1992**, 1112–1114.
9. Khan, A. R.; Barton, L.; D'Souza, V. T. *J. Org. Chem.* **1996**, *61*, 8301–8303.
10. Isac-Garcia, J.; Lopez-Paz, M.; Santoyo-Gonzalez, F. *Carbohydr. Lett.* **1998**, *3*, 109–116.
11. Khan, A. R.; Forgo, P.; Stine, K. J.; D'Souza, V. T. *Chem. Rev.* **1998**, *98*, 1977–1996.
12. Gattuso, G.; Nepogodiev, S. A.; Stoddart, J. F. *Chem. Rev.* **1998**, *98*, 1919–1958.
13. Kelly, D. R.; Mish'al, A. K. *Tetrahedron: Asymmetry* **1999**, *10*, 3627–3648.
14. Fujita, K.; Ohta, K.; Ikegami, Y.; Shimada, H.; Tahara, T.; Nogami, Y.; Koga, T.; Saito, K.; Nakajima, T. *Tetrahedron Lett.* **1994**, *35*, 9577–9580.
15. Harata, K.; Nagano, Y.; Ikeda, H.; Ikeda, T.; Ueno, A.; Toda, F. *J. Chem. Soc., Chem. Commun.* **1996**, 2347–2348.
16. Fujita, K.; Chen, W.-H.; Yuan, D.-Q.; Nogami, Y.; Koga, T.; Fujioka, T.; Mihashi, K.; Immel, S.; Lichtenthaler, F. W. *Tetrahedron: Asymmetry* **1999**, *10*, 1689–1696.
17. Ohta, K.; Fujita, K.; Shimada, H.; Ikegami, Y.; Nogami, Y.; Koga, T. *Chem. Pharm. Bull.* **1997**, *45*, 631–635.
18. Fujita, K.; Shimada, H.; Ohta, K.; Nogami, Y.; Nasu, K.; Koga, T. *Angew. Chem., Int. Ed. Engl.* **1995**, *34*, 1621–1622.
19. Nogami, Y.; Fujita, K.; Ohta, K.; Nasu, K.; Shimada, H.; Shinohara, C.; Koga, T. *J. Inclusion Phenom. Mol. Recognit. Chem.* **1996**, *25*, 57–60.

20. Nogami, Y.; Nasu, K.; Koga, T.; Ohta, K.; Fujita, K.; Immel, S.; Lindner, H. J.; Schmitt, G. E.; Lichtenthaler, F. W. *Angew. Chem., Int. Ed. Engl.* **1997**, *36*, 1899–1902.
21. Fujita, K.; Ohta, K.; Nogami, Y.; Nasu, K.; Shiratani, T.; Sudo, M.; Koga, T. In *Proceedings of the 9th International Symposium on Cyclodextrins, Santiago de Compostela, Spain, May* 31–*June* 3; Torres Labandeira, J. J.; Vila-Jato, J. L., Eds.; Kluwer Academic: Dordrecht/Boston, 1999; pp. 113–115.
22. Immel, S.; Fujita, K.; Lichtenthaler, F. W. *Chem. Eur. J.* **1999**, *5*, 3185–3192.
23. Yan, J.; Watanabe, R.; Yamaguchi, M.; Yuan, D.-Q.; Fujita, K. *Tetrahedron Lett.* **1999**, *40*, 1513–1514.
24. Fujita, K.; Tahara, T.; Sasaki, H.; Egashira, Y.; Shingu, T.; Imoto, T.; Koga, T. *Chem. Lett.* **1989**, 917–920.
25. Immel, S. In *Proceedngs of the* 10*th International Symposium on Cyclodextrins, May* 21–24; Szejtli, J., Ed.; Mia Digital Publishers: Ann Arbor, MI, 2000; pp. 274–281.
26. Koshland, Jr., D. E. *Angew. Chem., Int. Ed. Engl.* **1994**, *33*, 2475–2478.
27. Fujita, K.; Okabe, Y.; Ohta, K.; Yamamura, H.; Tahara, T.; Nogami, Y.; Koga, T. *Tetrahedron Lett.* **1996**, *37*, 1825–1828.
28. Lichtenthaler, F. W. *Angew. Chem., Int. Ed. Engl.* **1994**, *33*, 2364–2374.
29. Lichtenthaler, F. W.; Mondel, S. *Carbohydr. Res.* **1997**, *303*, 293–302.
30. Cuny, E.; Lichtenthaler, W.; Lindner, H. J. *Acta Crystallogr., Sect. C* **1994**, *50*, 1599–1601.
31. Brooks, B. R.; Bruccoleri, R. E.; Olafson, B. D.; States, D. J.; Swaminathan, S.; Karplus, M. *J. Comput. Chem.* **1983**, *4*, 187–217.
32. Nilsson, L.; Karplus, M. *J. Comput. Chem.* **1986**, *7*, 591–616.
33. Reiling, S.; Schlenkrich, M.; Brickmann, J. *J. Comput. Chem.* **1996**, *17*, 450–468.
34. Reiling, S.; Brickmann, J. *Macromol. Theory Simul.* **1995**, *4*, 725–743.
35. Connolly, M. L. *J. Appl. Crystallogr.* **1983**, *16*, 548–558.
36. Connolly, M. L. *Science* **1983**, *221*, 709–713.
37. Cremer, D.; Pople, J. A. *J. Am. Chem. Soc.* **1975**, *97*, 1354–1358.
38. Jeffrey, G. A.; Yates, J. H. *Carbohydr. Res.* **1979**, *74*, 319–322.
39. Lichtenthaler, F. W.; Immel, S. *Liebigs Ann.* **1996**, 27–37.
40. Wu, X.; Kong, F.; Lu, D.; Li, G. *Carbohydr. Res.* **1992**, *235*, 163–178.
41. Allen, F. H.; Bellard, S.; Brice, M. D.; Cartwright, B. A.; Doubleday, A.; Higgs, H.; Hummelink, T.; Hummelink-Peters, B. G.; Kennard, O.; Motherwell, W. D. S.; Rodgers, J. R.; Watson, D. G. *Acta Crystallogr., Sect. B* **1979**, *35*, 2331–2339.
42. Allen, F. H.; Kennard, O.; Taylor, R. *Acc. Chem. Res.* **1983**, *16*, 146–153.
43. Pozsgay, V.; Dubois, E. P.; Lotter, H.; Neszmelyi, A. *Carbohydr. Res.* **1997**, *303*, 165–173.
44. Lipkowitz, K. B.; Green, K.; Yang, J. A. *Chirality* **1992**, *4*, 205–215.
45. Saenger, W.; Jacob, J.; Gessler, K.; Steiner, T.; Hoffmann, D.; Sanbe, H.; Koizumi, K.; Smith, S. M.; Takaha, T. *Chem. Rev.* **1998**, *98*, 1787–1802.
46. Chacko, K. K.; Saenger, W. *J. Am. Chem. Soc.* **1981**, *103*, 1708–1715.
47. Van Gunsteren, W. F.; Berendsen, H. J. C. *Mol. Phys.* **1977**, *34*, 1311–1327.
48. Immel, S. *MOLARCH*$^{+}$: *Molecular Architecture Modeling Program V*6.15; Technical University of Darmstadt: Germany, 2001.
49. Sheldrick, G. M. *SHELXD*-97: *Program for Crystal Structure Solution of Macromolecules*; University of Göttingen: Germany, 2000.
50. Sheldrick, G. M. *SHELXL*-97: *Program for Crystal Structure Refinement*; University of Göttingen: Germany, 1997.